

Experimental Measurements of Starting Loads and Model Behaviors in the Indraft Supersonic Wind Tunnel*

By Ryojiro MINATO,¹⁾ Kazuhide MIZOBATA¹⁾ and Komei KUWATA²⁾

¹⁾*Aerospace Plane Research Center, Muroran Institute of Technology, Muroran, Japan*

²⁾*Department of Aerospace System Engineering, Graduate School of Muroran Institute of Technology, Muroran, Japan*

(Received April 27th, 2009)

Measurements of starting load in the indraft supersonic wind tunnel of Muroran Institute of Technology were conducted for Mach 2, 3 and 4 conditions with the AGARD-B model. The high-speed photographs covering the behaviors of the wind tunnel model from the start to end of the operation were taken. Those photographs make clear that the oscillations of the model coincide with the measured starting load oscillation and starting loads were caused by two shock waves. The first shock wave is the reflection shock, generated at the nozzle throat by expansion wave reflection. The second wave is comprised asymmetric oblique shock waves (AOS) coming from upstream. AOS can generate asymmetric conical shock (ACS) around the nose cone of the model, which would have directly caused the starting loads on the wind tunnel model. Based on these observations, propose a conical shock theory, as an alternative starting load prediction theory instead of the normal shock theory.

Key Words: Starting Loads, Supersonic Wind Tunnel, Aerodynamic Force Measurements

1. Introduction

The Aerospace Plane Research Center (APReC) at the Muroran Institute of Technology is studying aerospace transportation to promote fundamental technologies. Therefore, an indraft supersonic wind tunnel was rebuilt at APReC by reusing the nozzle blocks and major parts, from the blow-down supersonic wind tunnel at the University of Tokyo.

Aircraft movements consist of six degrees of freedom (6 DOF), and are governed by translational forces along the three mutually perpendicular axes and three rotational moments about these axes. In a wind tunnel test, these forces and moments are usually measured using a six-component internal balance, which is usually very expensive and requires careful handling, because it is easily damaged by excessive aerodynamic loads. To prevent damage, imposed loads on the wind tunnel model must be restricted to the balance limits. Aerodynamic loads can be divided into steady loads and starting loads. The former are objective loads in the wind tunnel tests and the latter are impulse forces caused by unsteady, transient flow at the beginning of tests. Starting loads are given more attention than steady loads for a balance safety. If the balance is designed to be sufficiently robustly to withstand to large starting loads, the sensitivity and resolution required for aerodynamic measurement cannot be guaranteed. Therefore, the model is either shielded by two retractable plates or inserted into the test section to reduce the starting loads.¹⁾ However, it is difficult to install such equipment in the present wind tunnel. In addition,

inevitable hatches or grooves on test section walls generate in undesirable shock waves.²⁾ The best method to prevent excess starting loads is to determine the model scale within the balance limit. Previously, starting loads have been predicted by normal shock theory, described in the next section. However, it is well known that this theory gives much larger starting loads value than actual values. Thus, the balance load limit is larger when starting load is evaluated by normal shock theory, leading to degraded measurement accuracy.

This study clarifies the factors governing starting load phenomena. Starting loads imposed on the AGARD-B model were measured in the APReC indraft supersonic wind tunnel at Muroran Institute of Technology. At the same time, we photographed of the model behavior with a high-speed video camera. We propose an alternative starting load prediction theory instead of the conventional shock theory.

2. Starting Load Theory from Previous Studies

Starting loads are thought to be caused by unsteady shock systems at the start of wind tunnel tests. Once a flow field established non-uniformly in the test section, an asymmetric shock system is formed around a model. Normal shock theory considers the asymmetric shock system as a normal shock wave. The normal shock stands at the front of the model on only one side and there is no shock exists on the other side. Therefore, the static pressure ratio between both sides is given by the normal shock relation.

$$\frac{p_2}{p_1} = 1 + \frac{2\gamma}{\gamma + 1} (M^2 - 1) \quad (1)$$

where, p_1 and p_2 are the static pressure fore and aft of the normal shock wave, respectively. p_1 , is considered to be a

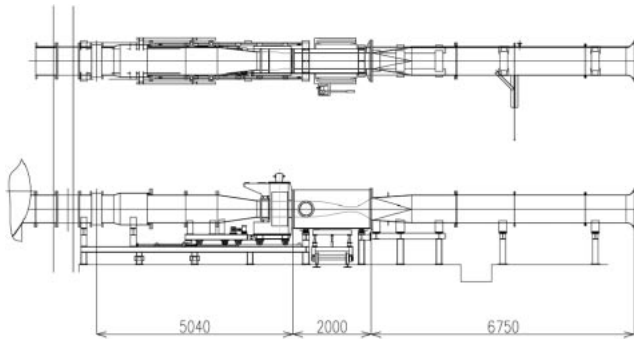


Fig. 1. Schematic of indraft supersonic wind tunnel in Muroran Institute of Technology.

static pressure at supersonic steady flow. M and γ are the airflow Mach number and the specific heat ratio. Thus, force acting on a model, F_{SL} , is evaluated by relation

$$F_{SL} = (p_2 - p_1)S$$

$$= \frac{2\gamma}{\gamma + 1} (M^2 - 1) \left(1 + \frac{\gamma - 1}{2} M^2 \right)^{\frac{\gamma}{\gamma - 1}} P_T S \quad (2)$$

where, P_T and S are the total pressure of airflow and the planform area of the model, respectively. The load coefficient C_N of the starting load non-dimensionalized by using two parameters P_T and S gives

$$C_N = \frac{F_{SL}}{P_T S} \quad (3)$$

The load coefficient for normal shock theory is defined by Eq. (4).

$$C_N = \frac{2\gamma}{\gamma + 1} (M^2 - 1) \left(1 + \frac{\gamma - 1}{2} M^2 \right)^{\frac{\gamma}{\gamma - 1}} \quad (4)$$

In the 1960s, many experimental studies were conducted to quantify the starting loads.^{3,4)} Based on these data, it was found that normal shock theory gives much larger values than experimental data. Therefore, Maydew introduced an empirical correction to normal shock theory.³⁾ Maydew's theory considers two cases of starting loads, with and without wings. It is fairer than normal shock theory and is widely accepted by researchers. However, some disagreements still remain between Maydew's theory and experimental data and it has reported that some experimental data exceed the theory's prediction,⁵⁾ because starting load is greatly dependent on the wind tunnel facilities and operations. Any alternative theory should include detailed flow conditions for adequate prediction.

3. Experimental Facility and Conditions

3.1. Indraft wind tunnel facility

A schematic of the APReC indraft supersonic wind tunnel at Muroran Institute of Technology is shown in Fig. 1. This facility was rebuilt in 2005 and has three nozzle sections generating Mach 2, 3 and 4 flows. It reuses parts from the intermittent blowdown supersonic wind tunnel at the University of Tokyo. Each nozzle block is on a rail truck with

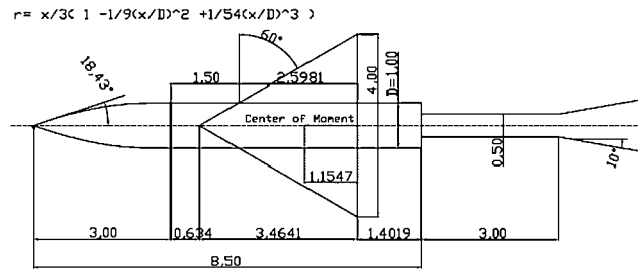


Fig. 2. Configuration of AGARD-B model.

hydraulic jacks. The nozzle block can be changed using jacks and a turntable. Each nozzle block has a test cross section of 400×400 (mm) and an axial length of 2000 mm. The configuration of the nozzle sections is 2D in the spanwise direction and divergent in the vertical direction from nozzle throats to the test sections. The details of nozzle configurations are described elsewhere.⁶⁾ Three vacuum tanks were located downstream of the wind tunnel. The volume of each tank is about 100 m^3 , giving, 300 m^3 in total. In 2009, five tanks were installed in this wind tunnel. Measurement times are about 10 s for Mach 2 and 3, and about 6 s for Mach 4. With an indraft wind tunnel, air moisture can cause frost in the test section during tests. This is undesirable for optical measurements. To prevent frost, an airbag to store dry air will be installed at the tunnel intake in future. Before each wind tunnel test, the vacuum tanks are evacuated to less than 5 kPa. The starting valve, which is installed between the test section and vacuum tanks, takes about 0.3 s from full close to full open. The airstream reaches a steady state within about 0.1 s after the starting valve is fully open.

3.2. Wind tunnel model (AGARD-B model)

This study used the AGARD-B model is to measure starting loads. It is the standard wind tunnel model to evaluate the quality of wind tunnel airflow. The configuration of the AGARD-B model is shown in Fig. 2 and is described in detail elsewhere.⁷⁾ The sizes of AGARD-B components are non-dimensionalized by its fuselage diameter, D . The fuselage diameter must be determined to keep the starting load within the load limits of the six-component internal balance. The balance used in this study has a lifting force limit of 245 N. The load coefficients of the starting load for the AGARD-B model. These load coefficients are measured in a blowdown supersonic wind tunnel and are non-dimensionalized by the dynamic pressure of the airflow and the planform area of the model. We reduced the load coefficients⁵⁾ to non-dimensional values in total pressure and obtained $C_N = 0.3$ under Mach 3 conditions as the maximum starting load. When the fuselage diameter is 24 mm, the starting load is 200.3 N, satisfying the balance limits. Thus, this study used the AGARD-B model with this determined fuselage diameter.

4. Experimental Methods

To clarify transient phenomena at the start of wind tunnel tests, we measured the unsteady lifting force (starting load)

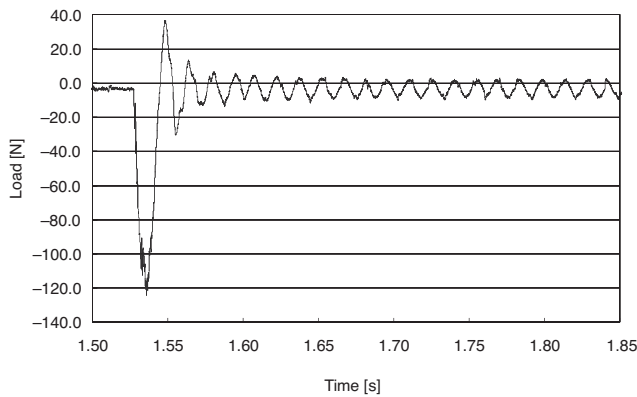


Fig. 3. Result of Hammering Test.

and static pressure on test section wall in this study. In addition, Schlieren photographs of model behavior and airflow around the model were taken using high-speed video camera. The time sequential data of starting load and wall pressure were stored in a PC at a 50-kHz sampling frequency using a 10-kHz LPF. A Hammering test was conducted to validate the sampling frequency and LPF conditions. In this test, the AGARD-B model was installed at the sting with the internal balance; this is a similar configuration to the wind tunnel tests. Figure 3 shows the result and indicates that the mechanical vibration of this system has a typical impulse response with 1 DOF and its natural frequency is 50 Hz. Therefore the sampling frequency and LPF conditions are adequate because the model is considered to oscillate with this frequency when starting loads or any other forces are imposed on it.

Wind tunnel test procedures are described below. The data for loads on the balance and wall pressure are saved to the PC about 3 s before the starting valve opens. The high-speed video camera started at about 2 s. When the high-speed video camera starts, a synchronous signal is sent to the PC to ensure the picture is synchronized with the data in the PC.

5. Results and Discussions

5.1. Starting loads and airflow Mach number

Wind tunnel tests were conducted under Mach 2, 3 and 4 conditions. Figure 4 shows the measured load coefficients of the starting loads measured as a function of Mach number. The results are compared with normal shock theory, Maydew's correlation and other experimental data.⁵⁾ At the three Mach number conditions, the load coefficients published in other research,⁵⁾ measured in a blowdown supersonic wind tunnel tend to be larger than our results. Some published data⁵⁾ are larger than the normal shock theory. Actual loads on a balance are proportional to the total pressure of airflow, so the indraft supersonic wind tunnel imposed less loads on the balance and less restriction on the design of the wind tunnel model than the blowdown tunnel. Commonly both indraft and blowdown supersonic wind tunnels exhibit maximum starting loads at around Mach 3 conditions. The

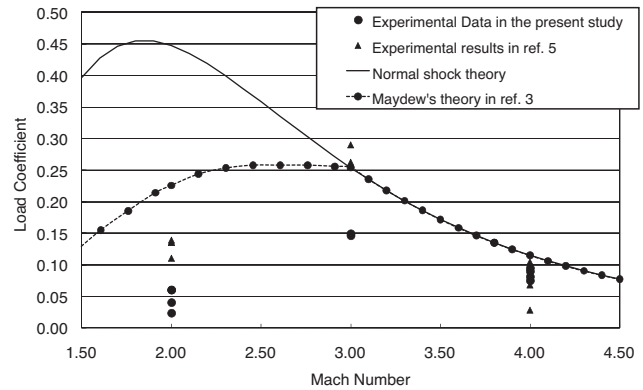


Fig. 4. Comparison of experimental load coefficients with normal shock theory.

starting loads for Mach 2 conditions are much lower than those predicted by normal shock theory, which predicts the maximum at Mach 1.84 as derived in Eq. (4). However, the experimental load coefficients in both the indraft and blowdown wind tunnel tests do not agree qualitatively with normal shock theory. Only at Mach 4 condition, both wind tunnel test data are close to normal shock theory, although the ejector system⁵⁾ was used at Mach 4 condition. Consequently, we conclude that normal shock theory does not explain actual starting load phenomena either quantitatively or qualitatively. We need an alternative theory to predict starting loads.

5.2. High speed video camera pictures

The time histories of the starting loads and wall static pressures at the start of wind tunnel tests are shown in Figs. 5 and 6 for the Mach 3 and 4 conditions, respectively. Both figures indicate that the transient durations from valve opening to steady flow last only 0.1 s at both Mach number conditions. The starting loads prior to steady state start at 0.2 s at maximum in our indraft wind tunnel tests. The published blowdown wind tunnel test⁵⁾ showed unsteady loads for about 1.0 s. The short durations of the indraft wind tunnel are advantageous in preventing damage to the balance.

From Figs. 5 and 6, the starting load oscillations at Mach 3 and 4 are composed of two main impulses. Two clear impulses are observed at 2.86 and 2.96 s at Mach 4. At Mach 3, the first oscillation is observed at about 1.05 s. This oscillation is damped and then enlarged again at about 1.11 s. The second oscillation is larger than the first. High-speed video pictures in Fig. 7 show a wave like dark shadow passing through the model before the first oscillation. Since our indraft wind tunnel has a starting valve between the test section and vacuum tanks, when the starting valve opens, an expansion fan propagates upstream from the vacuum tanks at first. The expansion fan reflects at the nozzle throat and returns to the vacuum tanks as a compression wave. The wave, which is going downstream, like the dark shadow captured in Fig. 7 may be the reflected compression wave. However, the expansion fan cannot be identified in these pictures, because its density variation is too small to identify. The AGARD-B model begins to oscillate after interaction with this reflected compression wave as shown

in Fig. 8. The oscillations of the model measured from the high-speed video pictures together with the starting load data are shown in Fig. 9. Although we tried to synchronize the recordings of the starting loads and pictures taken by the high speed video camera, we failed because there are uncertain delay times of about 0.04 to 0.1 s in the measurement system. Consequently, the time trace from the balance output is compared with the displacement of the model calculated from the video in Fig. 9 in order to match each other

in amplitude and phase. The same method was applied to the Mach 4 data shown in Fig. 10. We found that the oscillations in the high-speed video pictures do match with those of the starting load. This match indicates that the first oscillation at 1.05 s in Fig. 5 is caused by the reflected compression wave in Fig. 7. This proves that the rise in wall static pressure just before the first oscillation is due to the reflected compression wave.

Another rise in wall static pressure is also observed before the second oscillation. The high-speed video pictures in Fig. 11 show for the second oscillation. An asymmetric

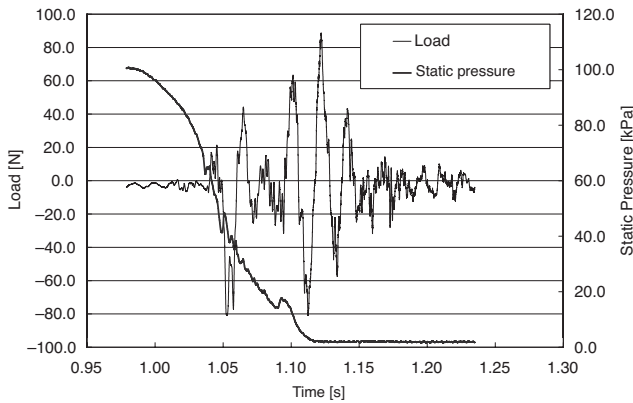


Fig. 5. Time histories of starting load and wall static pressure for Mach 3 condition.

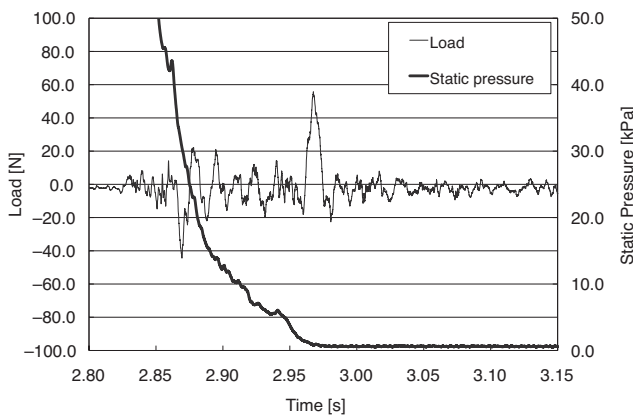


Fig. 6. Time histories of starting load and wall static pressure for Mach 4 condition.

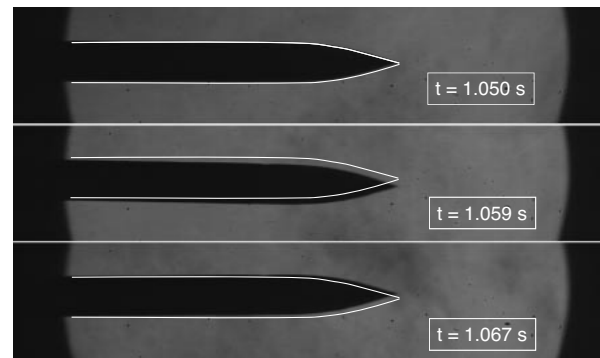


Fig. 8. Oscillation of AGARD-B model after reflected compression wave passage.

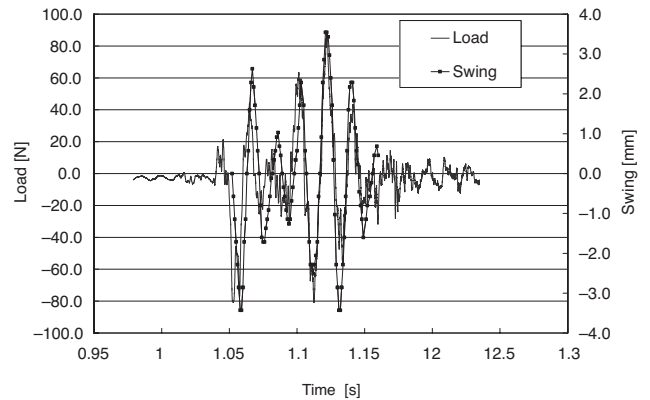


Fig. 9. Time histories of starting load and nose cone displacement for Mach 3 condition.



Fig. 7. Behavior of reflected compression wave for Mach 3 condition ($t = 1.036\text{--}1.038\text{ s}$).

oblique shock wave appears from upstream and interacts with the model, resulting in the second oscillation. The asymmetric conical shock wave is generated from the nose cone of the model after interaction with the asymmetric oblique shock wave. This asymmetric conical shock wave is believed to cause a pressure difference between the upper and lower sides of the model, generating the starting loads. The abatement of the second oscillation is more important for a wind tunnel test than abatement of the first oscillation because the second oscillation is larger than the first.

For the Mach 2 condition, the time history of the starting load and high-speed video picture are shown in Figs. 12 and 13. The starting load at Mach 2 condition is the lowest of the three Mach number conditions, corresponding to about 30% of that at Mach 3 conditions. For reproducibility, we conducted wind tunnel tests several times at given Mach number conditions, and some cases at Mach 2 cannot be identified as having distinct starting loads. The case in Fig. 12 has a clear starting load compared to other cases. The high-speed video picture at Mach 2 condition shows that the flow-field remains symmetrical during the transient period (from

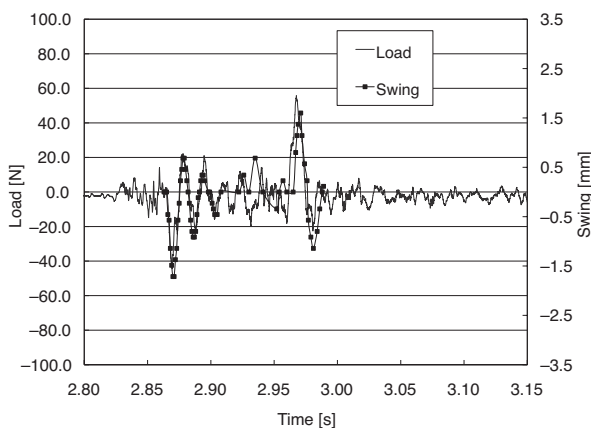


Fig. 10. Time histories of starting load and nose cone displacement for Mach 4 condition.

4.45 to 4.60 s in Fig. 12) and there is almost no oscillation of the model. This phenomenon clarifies that the asymmetric flow is related to generation of starting load. To confirm this, a test was conducted with the wing of the AGARD-B model vertical to the symmetric plane of the nozzle. In this configuration, the pressure difference caused by the asymmetric oblique shock wave is not imposed directly on the wing. The results are shown in Figs. 14 and 15 for Mach 3 and 4 conditions, respectively. The maximum starting load at Mach 3 with vertical wing is reduced to 40% of the load for horizontal case, and a similar reduction was observed for the Mach 4 condition. All nozzle blocks in at our facility are 2D and are divergent in the vertical direction. An asymmetric flowfield is formed in the vertical direction rather than the spanwise direction. Therefore, setting the wing vertical to the symmetric nozzle plane prevents the pressure difference between both wing sides. This method reduces the starting load as described in elsewhere.^{1,2)}

Asymmetric flows appear at Mach 3 condition, while Mach 2 flows are symmetric. It is unknown why the transition from symmetric to asymmetric flows occurs with increase in Mach number. A similar phenomenon is reported elsewhere.^{2,5)} The ostensible reason for asymmetric flows may depend on free-stream disturbances and an error in the geometric configuration at the nozzle throat. Even very low level flow disturbances can form an asymmetric flowfield. Since the width of the nozzle throat at low Mach number is relatively large, geometric error has less effect on flow uniformity near the throat and on the behavior of the boundary layer sensitive to flow disturbances. On the other hand, high Mach number conditions require a narrow nozzle throat, where geometric error leads readily to asymmetric flow in the test section.

As mentioned above, the asymmetric oblique shock wave from the nozzle produces the asymmetric conical shock wave around the model. To determine which shock waves generate starting load, the high-speed video pictures capturing detailed behaviors of the model at Mach 4 are shown in

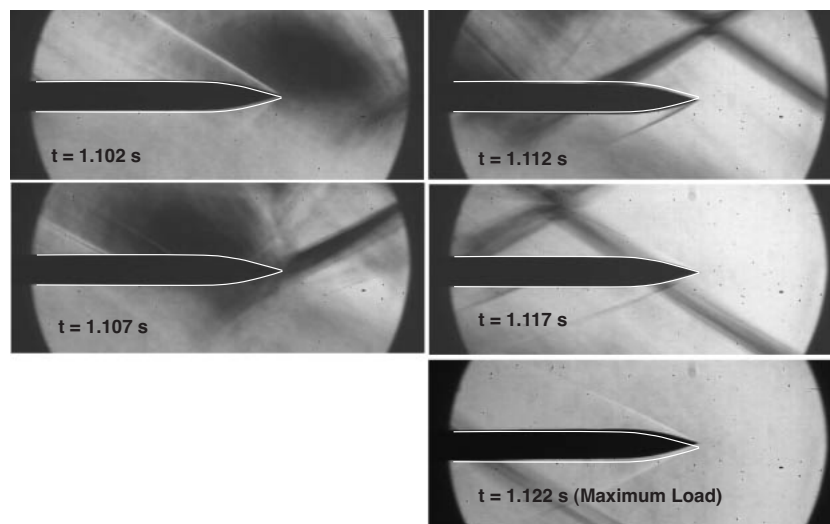


Fig. 11. Schlieren photography of asymmetric oblique shock wave for Mach 3 condition.

Fig. 16. First, the asymmetric oblique shock wave propagates downstream and interferes with the model. Then, the asymmetric conical shock is formed from the nose cone at 2.964 s. The model starts pitching oscillations after the asymmetric conical shock appears. Therefore, the asymmetric conical shock wave mainly generates the starting load.

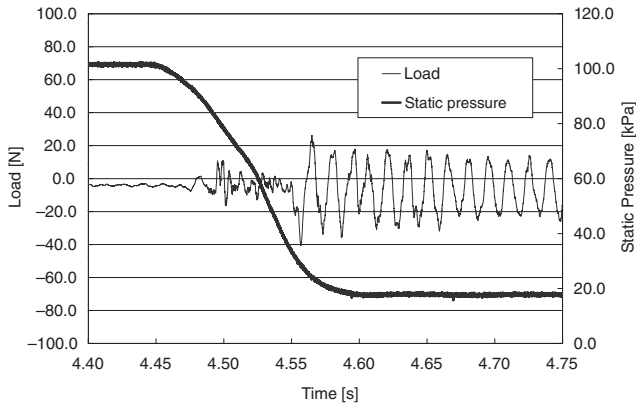


Fig. 12. Time histories of starting load and wall static pressure for Mach 2 condition.

5.3. Prediction by conical shock theory

The previous section explains that the asymmetric conical shock wave generates the starting loads. This asymmetric conical shock wave is generated when an asymmetric oblique shock wave interferes with the model. Normal shock theory explains that normal shock stands at the nose cone of the model only on one side and the pressure difference between both sides is evaluated by the normal shock relation. This pressure difference at evaluation has sometime overestimated starting loads. On the other hand, a static pressure upstream of the shock wave is evaluated as the static pressure at steady flow. However, the static pressure of the asymmetric oblique shock is larger than that at steady flow. For example, at the present Mach 3 condition, the former is about 18.0 kPa and the latter is 2.75 kPa. This indicates that normal shock theory might underestimate starting loads.

Based on these observations, we propose an alternative theory, called as conical shock theory to predict starting load. In place of the normal shock relation, the pressure difference is calculated by the conical shock relation

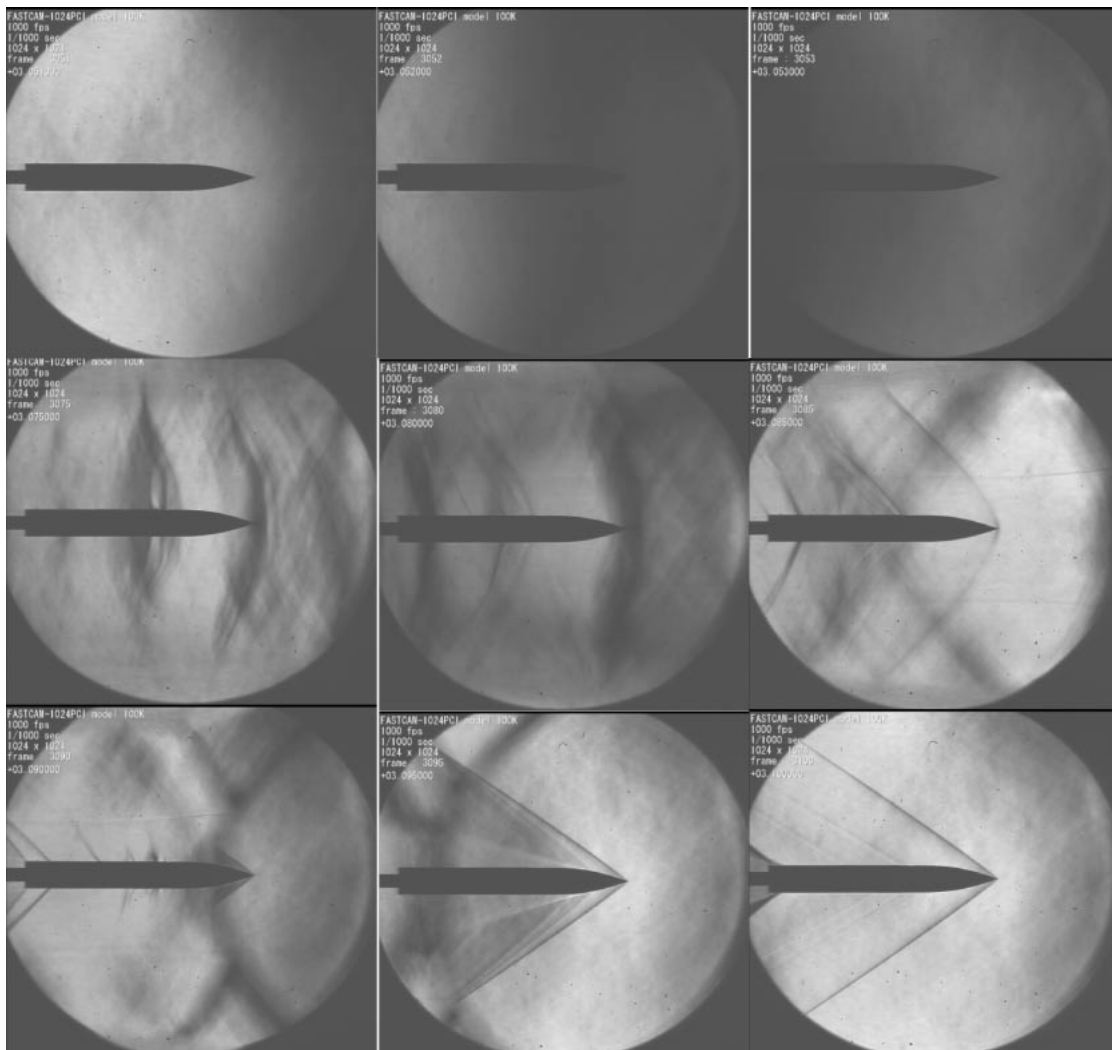


Fig. 13. Schlieren photograph of transient flowfield for Mach 2 condition.

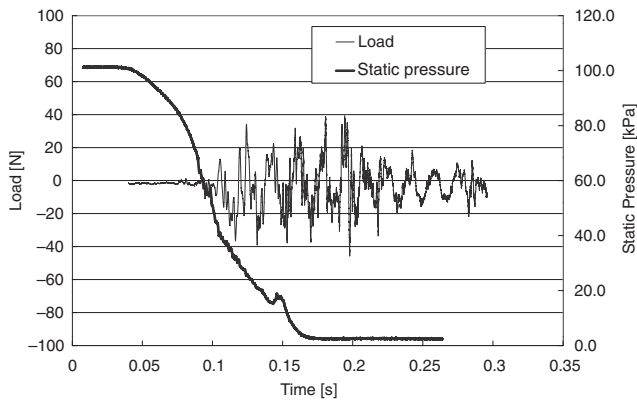


Fig. 14. Time histories of starting load and wall static pressure for Mach 3 condition and vertical wing.

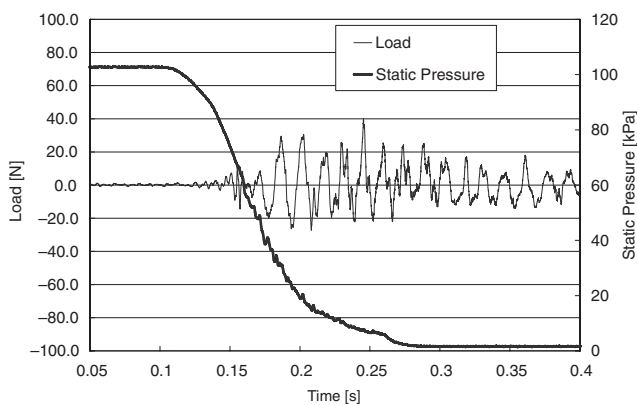


Fig. 15. Time histories of starting load and wall static pressure for Mach 4 condition and vertical positioned wing.

$$F_{SL} = p_1 S \frac{2\gamma}{\gamma + 1} (M^2 \sin^2 \beta - 1). \quad (5)$$

The load coefficient for the conical shock theory is given by dividing by planform area, S and total pressure of airflow, P_T , and can be expressed as Eq. (6)

$$C_N = \frac{p_1}{P_T} \frac{2\gamma}{\gamma + 1} (M^2 \sin^2 \beta - 1). \quad (6)$$

where, M and β are the Mach number of airflow and the angle of shock wave, respectively.

The static pressure, p_1 in Eq. (5) is equal to that of the asymmetric oblique shock wave and is unique to a wind tunnel facility. However, it does not depend on the wind tunnel model. As a result, p_1 should be given experimentally before the objective aerodynamic test. For an axisymmetric slender body like the AGARD-B model, β can be determined by solving the Taylor-Maccoll equation.⁸⁾ For a 2D model, β is given by the oblique shock relation. For other configurations, it is difficult to determine β theoretically, although we suggest that CFD solution for steady flow might yield β . As known in Eq. (5), the static pressure over the subsonic side is equal to the pressure behind the conical shock. The conical shock relation dictates that the pressure behind the shock is smaller than the static pressure on the cone surface. If the theoretical cone surface pressure is

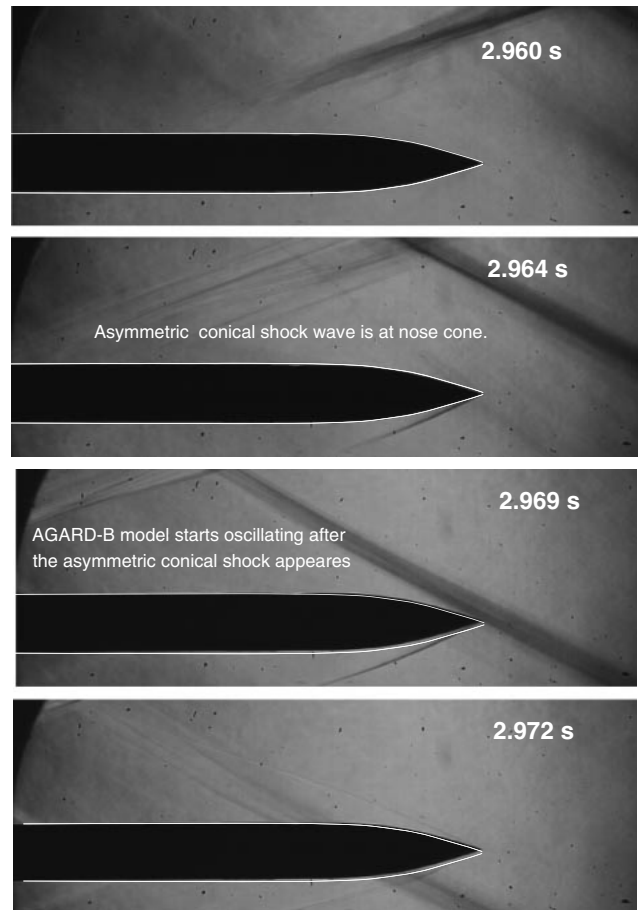


Fig. 16. Schlieren photograph of asymmetric conical shock wave with AGARD-B model.

imposed on the entire planform area of the model, the starting loads would be larger than those predicted by the conical shock theory. However, such a situation may be unrealistic for the reason described below. An axisymmetric slender body like the AGARD-B model has convex streamlines along its surface from cone to fuselage and an expansion fan can be generated from there. The surface pressure on the fuselage is reduced by the expansion fan from shoulder of the model.

By using experimental data and the Taylor-Maccoll equation, the constants for Eq. (5) are given as follows.

$$\begin{aligned} \text{Mach 2, } & \beta = 36.470 \text{ deg, } p_1 = 33.6 \text{ kPa} \\ \text{Mach 3, } & \beta = 28.179 \text{ deg, } p_1 = 18.2 \text{ kPa} \\ \text{Mach 4, } & \beta = 24.960 \text{ deg, } p_1 = 6.87 \text{ kPa} \end{aligned}$$

For Mach 2, no asymmetric oblique shock or pressure rise is observed in Figs. 12 or 13. Thus, at Mach 2, p_1 is evaluated for the static pressure value just before the starting load oscillation appears. The planform area, S , is 66.22 cm^2 . The load coefficients for the conical shock theory are compared with the previous theories in Fig. 17. The conical shock theory agrees qualitatively with the experiment at all Mach number conditions. The experimental starting load is 70% of the conical shock theory prediction for the Mach 3 condition and 60% for the Mach 4. Some quantitative errors still remained between theory and experiment. However, the

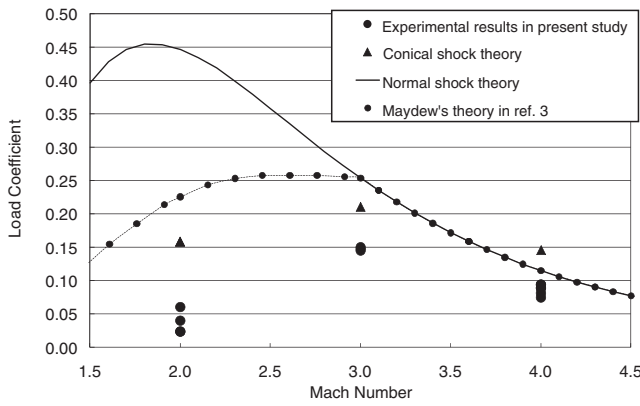


Fig. 17. Comparison of experimental load coefficients with conical shock theory.

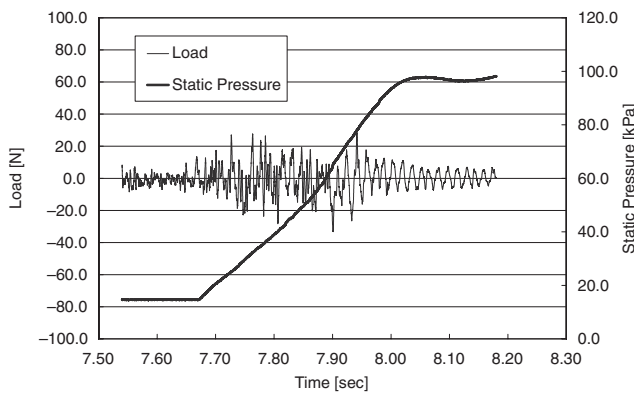


Fig. 18. Time histories of load and wall static pressure for Mach 2 condition at end of testing.

conical shock theory predicts larger values than the experimental data and gives a margin for the actual load. Therefore, the conical shock theory is a useful and practical design tool for the wind tunnel model.

5.4. Transient load at end of wind tunnel test

In addition to the starting load, an unsteady, transient load is imposed on the wind tunnel model at the test end. Other work²⁾ reports that this load is the same level as the starting load. We investigated the transient load at the test end for all Mach numbers. Figures 18 and 19 show the time histories for the wall static pressures and starting loads for Mach 2 and 3. In our experiments, the loads at the test end are about half the maximum starting loads at Mach 3 and 4. At Mach 2, the end load is the same as the starting load. Therefore, the prediction by the conical shock theory is 30% or 40% more than the experimental data and reasonable for designing the wind tunnel model. Future work will validate the conical shock theory for other wind tunnel facilities and flow conditions. Further investigation of the mechanisms and flow phenomena concerning these transient loads also remains to be done.

6. Conclusions

The starting loads imposed on the AGARD-B model were investigated using the indraft supersonic wind tunnel at

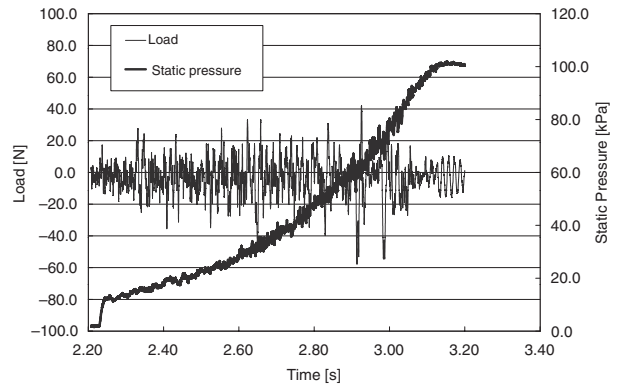


Fig. 19. Time histories of load and wall static pressure for Mach 3 condition at end of testing.

Muroran Institute of Technology. The conclusions are summarized below.

1. The starting loads in the indraft supersonic wind tunnel are composed of two impulses. The first impulse is generated by the reflected compression wave, which is caused by the initial expansion fan. The second impulse is generated by the asymmetric oblique shock wave. The load imposed by the second impulse is larger than the first.

2. The amplitude of measured starting loads coincides with the model oscillation appearing in the high-speed video pictures. Therefore, there is similarity between the starting load data and video pictures at Mach 3 and 4 conditions.

3. Asymmetric oblique shock waves are generated at high Mach numbers and generate large starting loads. On the other hand, at Mach 2 condition, the flowfield is symmetric resulting in lower starting loads. If the model wing is set vertical to the nozzle symmetric plane at Mach 3, the starting load is reduced dramatically to 40% of the load at horizontal position. Therefore, the asymmetric shock wave governs starting load generation.

4. In the high-speed video pictures, model loads are seen to be caused by the asymmetric conical shock wave, generated by interference between asymmetric oblique shock waves and the model. The model starts oscillating after the asymmetric conical shock wave is generated from its nose cone. Thus, the asymmetric conical shock wave creates the pressure difference between the model upper and lower sides.

5. A conical shock theory is proposed. Its predictions are about 70% and 60% of the experimental values at Mach 3 and 4 conditions, respectively. The conical shock theory can be applied to a wind tunnel model because it reasonably explains the trend in the starting load coefficients with sufficient margin to assure balance safety.

Acknowledgments

Finally, we would like to express our thanks to Prof. Nobuhiko Tanatsugu and Kazuyuki Higashino at APReC for their fruitful discussions and comments.

References

- 1) Pope, A. and Goin, K. L.: *High Speed Wind Tunnel Testing*, Robert, E., ed., Krieger Publishing Company, Malabar, Florida, 1965, pp. 365–369.
- 2) Iijima, H., Watanabe, M., Kanda, H., Sato, M., Nagai, S. and Suzuki, N.: Effects of Several Parameters on Starting/Stopping Loads in Supersonic Wind Tunnels, JAXA Research and Development Report, JAXA-RR-05-048, 2006 (in Japanese).
- 3) Maydew, R. C.: *Compilation and Correlation of Model Starting Loads from Several Supersonic Tunnels*, Sandia Corporation-4691 (RR), 1962.
- 4) Crane, J. F. W. and Woodley, J. G.: The 7 in. \times 7 in. Hypersonic Wind Tunnel at R.A.E. Farnborough, Part IV—Measurements of Diffuser Performance, Blockage, Starting Loads and Humidity, Aeronautical Research Council Current Papers, No. 663 1963.
- 5) Irikado, T., Sato, K. and Fujii, K.: Transient Loads and Flow Structures in the ISAS Supersonic Wind Tunnel, Proceedings of the 38th Fluid Dynamics Conference, Muroran, 2006, pp. 259–262 (in Japanese).
- 6) Committee for Building of Supersonic Wind Tunnel Facility: Report on Building of Supersonic Wind Tunnel Facility, Report of Institute of Aeronautic Science, University of Tokyo, No. 3, 1962–1963, pp. 477–479 (in Japanese).
- 7) Bromm, A. F., Jr.: Investigation of Lift, Drag and Pitching Moment of a 60 deg Delta-Wing-Body Combination (AGARD Calibration Model B) in the Langley 9-inch Supersonic Tunnel, NACA TN-3300, 1954.
- 8) Shapiro, A. H.: *The Dynamics and Thermodynamics of Compressible Fluid Flow*, The Ronald Press Company, New York, 1953, pp. 651–663.